Available online at www.sciencedirect.com

ScienceDirect

Advances in Space Research 61 (2018) 74–88

ADVANCES IN SPACE RESEARCH (a COSPAR publication)

www.elsevier.com/locate/asr

Improving magnetosphere in situ observations using solar sails

Khashayar Parsay [a,*], Hanspeter Schaub [a], Conrad Schiff [b], Trevor Williams [b]

[a] Aerospace Engineering Sciences Department, University of Colorado, Boulder, CO 80309-0431, USA
[b] NASA Goddard Space Flight Center, 8800 Greenbelt Road, Greenbelt, MD 20771, USA

Received 27 April 2017; received in revised form 12 July 2017; accepted 31 July 2017
Available online 9 August 2017

Abstract

Past and current magnetosphere missions employ conventional spacecraft formations for in situ observations of the geomagnetic tail. Conventional spacecraft flying in inertially fixed Keplerian orbits are only aligned with the geomagnetic tail once per year, since the geomagnetic tail is always aligned with the Earth-Sun line, and therefore, rotates annually. Solar sails are able to artificially create sun-synchronous orbits such that the orbit apse line remains aligned with the geomagnetic tail line throughout the entire year. This continuous presence in the geomagnetic tail can significantly increase the science phase for magnetosphere missions. In this paper, the problem of solar sail formation design is explored using nonlinear programming to design optimal two-craft, triangle, and tetrahedron solar sail formations, in terms of formation quality and formation stability. The designed formations are directly compared to the formations used in NASA's Magnetospheric Multi-Scale mission.
Published by Elsevier Ltd on behalf of COSPAR.

Keywords: Solar sail; Formation flying; Magnetosphere mission; Heliophysics

1. Introduction

Many magnetosphere missions require more than a single spacecraft to achieve their scientific objective. National Aeronautics and Space Administration's (NASA) Time History of Events and Macroscale Interactions during Substorms (THEMIS), Magnetospheric Multi-Scale (MMS), and Radiation Belt Storm Probes (RBSP) missions, along with European Space Agency's (ESA) Cluster II mission are some of the currently active magnetosphere missions requiring multiple spacecraft to accomplish their scientific objectives. THEMIS was launched in February 2007 with the main scientific objective of studying auroras. It initially comprised of five spacecraft. The THEMIS mission confirmed that auroras are triggered by magnetic reconnection. Two of the THEMIS probes are now in lunar orbits forming the Acceleration, Reconnection, Turbulence and Electrodynamics of Moon's Interaction with the Sun (ARTEMIS) mission. These two probes study the effects of the Sun's radiation on the Moon in the absence of a magnetic field to shield it. The Cluster II mission was launched in July 2000 in order to study the dayside of the magnetosphere in three dimensions over an entire solar cycle of 11 years. Cluster II uses four identical spinning spacecraft that form a tetrahedron around the orbit apogee of a 4 $R_E \times 19.6$ R_E reference orbit with an inclination of 135°.

Generally, exploring the Earth's magnetic environment in three dimensions requires multiple satellites to fly in formation. NASA launched the MMS mission in Mar 2015 to study the three-dimensional structure of magnetic reconnection using four identical spinning spacecraft in order to separate the temporal and spatial plasma variations. The spacecraft form a regular tetrahedron formation within a specified region of interest around orbit apogee.

* Corresponding author.
E-mail addresses: khashayar.parsay@colorado.edu (K. Parsay), hanspeter.schaub@colorado.edu (H. Schaub), conrad.schiff-1@nasa.gov (C. Schiff), trevor.w.williams@nasa.gov (T. Williams).

http://dx.doi.org/10.1016/j.asr.2017.07.045
0273-1177/Published by Elsevier Ltd on behalf of COSPAR.

Nomenclature

$\boldsymbol{r}$	sail position vector [km]
μ	Earth's gravitational constant [km^3/s^2]
$\boldsymbol{a}_s$	solar radiation pressure acceleration [km/s^2]
$\boldsymbol{a}_\oplus$	acceleration due to Earth's nonsphericity [km/s^2]
$\boldsymbol{a}_\leftmoon$	acceleration due to moon's gravity [km/s^2]
$\boldsymbol{a}_\odot$	acceleration due to sun's gravity [km/s^2]
$\hat{\boldsymbol{n}}_s$	Sun-line unit vector
$\hat{\boldsymbol{n}}$	sail normal unit vector
a_r, a_θ, a_h	solar radiation pressure acceleration along radial, along-track, and cross-track direction [km/s^2]
$\boldsymbol{\text{œ}}$	array containing classical orbital elements $[a, e, i, \Omega, \omega, f]^T$. a: semi-major axis [km], e: eccentricity, i: inclination [rad], Ω: right ascension of ascending node [rad], ω: argument of perigee [rad], f: true anomaly [rad]
k	characteristic acceleration of solar sail [km/s^2]
$\boldsymbol{\rho}$	relative position vector between spacecraft [km]
ρ	inter-spacecraft range [km]
$Q(t)$	instantaneous metric to evaluate formation quality
$\overline{Q}_{\text{RoI}}$	average quality factor over a single orbit
$A(t)$	instantaneous area of a triangle formation
$V(t)$	instantaneous volume of a tetrahedron formation
$[\boldsymbol{C}_i]$	rotation matrix about the i axis
$\mathcal{O}$	local-vertical-local-horizontal (LVLH) frame
$\mathcal{N}$	Earth-centered inertial frame
$[\mathcal{NO}]$	direction cosine matrix that transfers a vector from $\mathcal{O}$ to $\mathcal{N}$ frame
λ_s	Sun longitude measured from vernal equinox [rad]

Subscript

c	denotes the chief solar sail
d	denotes the deputy solar sail
j	denotes spacecraft number in formation

Acronym

SRP	solar radiation pressure
R_E	Earth radius
RoI	science region of interest
NLP	nonlinear programming

The MMS mission has two primary science phases. In the first phase, the formation flies in a 1.2 $\text{R}_\text{E} \times 12\ \text{R}_\text{E}$ orbit, with the apogee lying inside the dayside of the magnetosphere. In the second phase, the orbit apogee is raised from 12 R_E to 25 R_E, with the orbit apogee lying within the nightside of the magnetosphere. The duration of both science phases are less than six months because of MMS's inertially fixed orbits. Since the exact location of the magnetic reconnection is unknown and, more importantly, varies with Sun activity, the tetrahedron formation must change its size, ranging from 400 km to 7 km in terms of averaged side length. The Earth's magnetic tail is directed along the Sun-Earth line and therefore rotates annually. Conventional magnetosphere missions require a highly elliptical orbit with its apogee inside the geomagnetic tail. The placement of the orbit apogee within a specific region of interest allows for the maximization of time the spacecraft spends in that region. An inertially fixed orbit is aligned with the geomagnetic tail only once a year, which limits the continuous presence and duration of the science phase to less than three months. Solar sail low-thrust propulsion, however, is capable of achieving long residence times in the geomagnetic tail by continuously precessing the orbit apse line, as illustrated in Fig. 1 (McInnes et al., 2001; Macdonald and McInnes, 2005; Macdonald et al., 2007). Note that in this paper, when an orbit is referred to as Sun-synchronous, it should not be confused with a conventional Sun-synchronous orbit whose precession rate of longitude of ascending node equals the mean motion of the Earth about the Sun. Solar sail formation flying in Earth-centered Sun-synchronous orbits for exploring the magnetosphere are studied in Gong et al. (2011) and Mu et al. (2014), using active control. In these studies, both linear and nonlinear controllers are applied by the deputy spacecraft to maintain circular projected relative orbits about the chief. The formation designed in this paper takes a completely different approach, namely natural formation

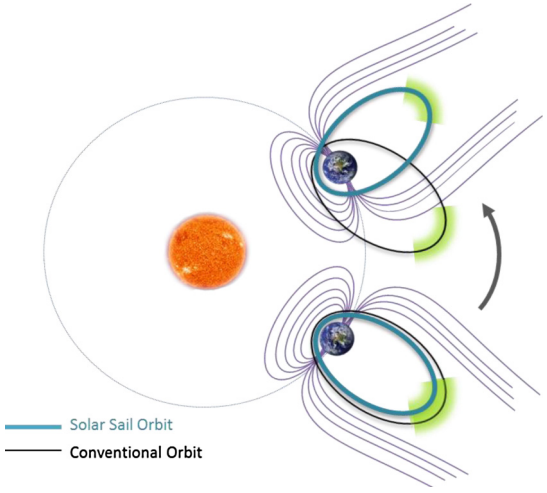

Fig. 1. Comparison of chemical and solar Sail propulsion in geomagnetic tail exploration.

flying, where all solar sails in formation maintain a fixed or unsteered Sun-pointing attitude solely for the purpose of precessing their orbit apse lines Sun-synchronously. In other words, once the formation is initialized, the sails need to only maintain their sun-pointing attitude.

At this point it should be emphasized that important heliophysics science can be achieved with two-craft (Van Allen Probes and ARTEMIS), three-craft (THEMIS), and four-craft (MMS and Cluster II) formations. The key component is adapting the location of the center of the formation and the spacing of the spacecraft to match the location and size of the plasma processes of interest. Achieving these conditions enables coordinated measurements to separate temporal and spatial variations. Perhaps the most intriguing application of Sun-synchronous sail orbit technology is to have continuous coverage in the geomagnetic tail where wave-particle interactions precipitate high energy magnetospheric electrons into the ionosphere.

Precipitating high-energy (600–10,000 eV) electrons are the source of ionization of neutral gas atoms (Evans and Moore, 1979) in the upper atmosphere and one of the two most commonly conceived mechanisms for atmospheric escape (Strangeway et al., 2005; Moore and Khazanov, 2010). These electrons, which are trapped on closed magnetic field lines whose footprints essentially terminate in the ionosphere, can bounce back and forth between their northern and southern boundaries, leaving secondary electrons and ionized gas in their wake. The ionized gas can then be accelerated up into the magnetosphere and potentially can leave the Earth completely. The secondary electrons are available to create new ionizations and further the outflow process.

These precipitating electrons are thought to originate in the tailside of the magnetosphere where they are scattered into their bounce trajectories by their interaction with Whistler chorus waves (Khazanov et al., 2015). Since the magnetotail has been only partially explored on those occasions, when previous spacecraft missions have naturally passed through it for approximately 2–3 months during each year, the resonances and excitations of the wave-particle interactions are poorly understood.

Having a formation with the usual complement of fields (fluxgate magnetometer), waves (Langmuir probes for electric field and search coil magnetometer), and particle (electrostatic spectrometers) sensors *parked* in the geomagnetic tail would provide near-continuous monitoring of the wave-particle interaction and would shed light on the important geophysical process of atmospheric outflow.

This paper aims to explore the possibility of *solar sail formation flying* in Earth-centered, Sun-synchronous orbits that would allow a formation to remain in the geomagnetic tail throughout the entire year as opposed to the few months achieved using conventional spacecraft, such as the ones used in the MMS mission. This paper is organized as follows. Section 2 reviews how a solar sail may be used to artificially precess the orbit apse line Sun-synchronously. Section 3 explores the problem of solar sail formation design in detail for various formation sizes and shapes. The designed solar sail formations are directly compared to the formations used in MMS mission in terms of formation quality and stability. Concluding remarks are given in Section 4.

2. Equations of motion of solar sails in Earth orbits

The general equations of motion for a solar sail in an Earth orbit is written as:

$$\ddot{\boldsymbol{r}} = -\frac{\mu}{r^3}\boldsymbol{r} + \boldsymbol{a}_{\oplus} + \boldsymbol{a}_{\leftmoon} + \boldsymbol{a}_{\odot} + \boldsymbol{a}_s \tag{1}$$

where $\boldsymbol{r}$ is the position vector of the spacecraft relative to the Earth and $\boldsymbol{a}_{\oplus}$, $\boldsymbol{a}_{\leftmoon}$, $\boldsymbol{a}_{\odot}$, and $\boldsymbol{a}_s$ are the accelerations due to Earth's nonsphericity, lunar gravitational effects, solar gravitational effects, and solar radiation pressure respectively. The adopted inertial frame $\mathcal{N} = \{O, \boldsymbol{X}, \boldsymbol{Y}, \boldsymbol{Z}\}$ has its origin O at the center of the Earth where the $\boldsymbol{X}$ axis points from the origin to the vernal equinox and $\boldsymbol{Z}$ points along the ecliptic north pole. The $\boldsymbol{Y}$ axis completes the right-handed coordinate system. For a flat, rigid, perfectly reflecting solar sail, the solar sail's acceleration due to the SRP can be written as

$$\boldsymbol{a}_s = k(\hat{\boldsymbol{n}}_s \cdot \hat{\boldsymbol{n}})^2 \hat{\boldsymbol{n}} \tag{2}$$

where $\hat{\boldsymbol{n}}$ is a unit vector normal to the sail surface, $\hat{\boldsymbol{n}}_s$ is a unit vector from the Sun to the Earth, and the parameter k is the sail's characteristic acceleration, which is defined as the acceleration experienced by the solar sail at a heliocentric distance of 1 astronomical unit (au) while the sail normal is directed along the sun-line (McInnes, 2004). For the GEOSAIL mission, McInnes and Macdonald propose flying a solar sail in the ecliptic plane using a simple steering law consisting of the sail's normal vector continuously pointing along the Sun-line within the orbit plane such that the rotation of the orbit apse-line is synchronous with the annual rotation of the Sun-line (McInnes et al., 2001; Macdonald and McInnes, 2005; Macdonald et al., 2007). The Sun-synchronized precession of the orbit apse-line allows the orbit apogee to remain in the geomagnetic tail continuously, thus enabling science data collection for long periods. The required characteristic acceleration k to precess the orbit Sun-synchronously is dependent on the shape of the orbit and is computed according to McInnes et al. (2001) and Macdonald et al. (2007)

$$k(a,e) = \frac{2}{3}\dot{\lambda}_s \frac{e}{\sqrt{1-e^2}}\sqrt{\frac{\mu}{a}} \tag{3}$$

where a and e are the orbit semi-major axis and eccentricity, respectively. The constant $\dot{\lambda}$ is the rate of change of Sun's longitude, which is assumed to be 0.9856 deg per day. To describe the $\hat{\boldsymbol{n}}$ vector resulting from the Sun-pointing steering law in the inertial frame $\mathcal{N}$, a local

reference frame must be defined. Let $\mathcal{O} = \{o, \hat{\boldsymbol{o}}_r, \hat{\boldsymbol{o}}_\theta, \hat{\boldsymbol{o}}_h\}$ define the sail's local-vertical-local-horizontal (LVLH) reference frame with its origin point o at the sail's center of mass, where $\hat{\boldsymbol{o}}_r$ points along the sail's position vector, $\hat{\boldsymbol{o}}_h$ is directed along the orbit angular momentum vector, and $\hat{\boldsymbol{o}}_\theta = \hat{\boldsymbol{o}}_h \times \hat{\boldsymbol{o}}_r$ completes the right-handed coordinate system. In this paper, all the computed relative position vectors ${}^{\mathcal{O}}\boldsymbol{\rho} = x\hat{\boldsymbol{o}}_r + y\hat{\boldsymbol{o}}_\theta + z\hat{\boldsymbol{o}}_h$ as well as the relative motion trajectories are expressed in the chief's LVLH frame.

As shown in Fig. 2(a), the α and ϕ angles track the orientation of the sail's normal with respect to the $\mathcal{O}$ frame. Thus, the sail's normal vector is expressed in the $\mathcal{O}$ frame as

$$ {}^{\mathcal{O}}\hat{\boldsymbol{n}} = \begin{bmatrix} \cos\alpha\cos\phi \\ \cos\alpha\sin\phi \\ -\sin\alpha \end{bmatrix}^{\mathcal{O}} \tag{4} $$

where the left-superscript $\mathcal{O}$ indicates the frame that the sail's normal $\hat{\boldsymbol{n}}$ is expressed in. As illustrated in Fig. 2(b), the sail's normal $\hat{\boldsymbol{n}}$ points along the Sun-line within the ecliptic plane such that the identities $\omega = \lambda_s$ and $\hat{\boldsymbol{n}} \cdot \hat{\boldsymbol{n}}_s = 1$ hold. This leads to orbit apse-line always pointing along the sun-line $\hat{\boldsymbol{n}}_s$. The SRP acceleration $\boldsymbol{a}_s$ expressed in the LVLH frame may be written as

$$ {}^{\mathcal{O}}\boldsymbol{a}_s = k(\hat{\boldsymbol{n}}_s \cdot \hat{\boldsymbol{n}})^2 {}^{\mathcal{O}}\hat{\boldsymbol{n}} = \begin{bmatrix} a_r \\ a_\theta \\ a_h \end{bmatrix}^{\mathcal{O}} = \begin{bmatrix} k\cos\alpha\cos\phi \\ k\cos\alpha\sin\phi \\ -k\sin\alpha \end{bmatrix}^{\mathcal{O}} $$

The sail's assumed orientation results in having $\phi = \pi - f$ and $\alpha = 0$. Substituting these identities to Eq. (4), the sail's normal vector may be further simplified to

$$ {}^{\mathcal{O}}\hat{\boldsymbol{n}} = \begin{bmatrix} -\cos f \\ \sin f \\ 0 \end{bmatrix}^{\mathcal{O}} \tag{5} $$

The direction cosine matrix $[\mathcal{NO}] = \left[{}^{\mathcal{N}}\hat{\boldsymbol{o}}_r\, {}^{\mathcal{N}}\hat{\boldsymbol{o}}_\theta\, {}^{\mathcal{N}}\hat{\boldsymbol{o}}_h\right]$ is used to transfer the sail's normal ${}^{\mathcal{O}}\hat{\boldsymbol{n}}$ from the reference frame $\mathcal{O}$ to the inertial frame $\mathcal{N}$ to be used in Eq. (1). Thus the sail's normal expressed in the $\mathcal{N}$ frame is

$$ {}^{\mathcal{N}}\hat{\boldsymbol{n}} = [\mathcal{NO}]\, {}^{\mathcal{O}}\hat{\boldsymbol{n}} \tag{6} $$

The sunlight direction expressed in the inertial frame $\mathcal{N}$ can be written as

$$ {}^{\mathcal{N}}\hat{\boldsymbol{n}}_s = \begin{bmatrix} -\cos\lambda_s \\ -\sin\lambda_s \\ 0 \end{bmatrix}^{\mathcal{N}} \tag{7} $$

where the longitude of the Sun λ_s is determined through

$$ \lambda_s = \lambda_{s_0} + \dot{\lambda}_s t \tag{8} $$

Finally, the SRP acceleration ${}^{\mathcal{N}}\boldsymbol{a}_s$ is determined by substituting Eqs. (6) and (7) into Eq. (2). The mission orbit considered in this paper is a 11 $R_E \times 30R_E$ orbit that lies in the ecliptic plane, where the perigee is placed in the planetary day-side and the apogee is aligned with the geomagnetic tail. Note that many interesting magnetospheric phenomenan such as magnetic reconnection occur on the night-side of Earth between 20 R_E and 30 R_E (Curtis,

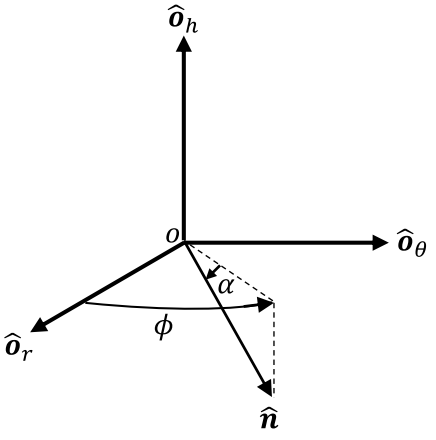

(a) Sail's normal vector orientation in the LVLH frame

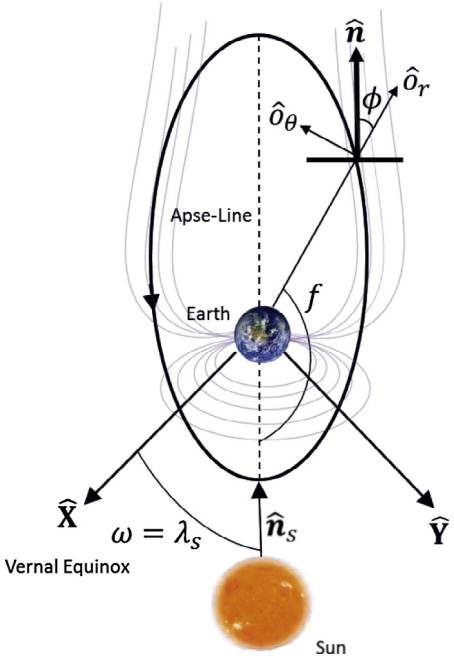

(b) Solar sail geometry in Sun-synchronous orbit

Fig. 2. Sail's orbit geometry and general orientation.

1999). The corresponding orbit period is $T = 5.4457$ days. The orbital elements for the mission orbit are $a = 130751.8$ km, $e = 0.4634$, $i = 0$ deg, $\omega = 0$ deg, and $\Omega = 0$ deg.

3. Solar sail formation flying

The science region of interest (RoI) for exploring the geomagnetic tail is shown in Fig. 3. In this paper, the region of interest is defined as all portions of the chief's orbit with distance above 21 R_E. The objective is to design formations that achieve their desired size and shape within this specified region of interest around apogee. Depending on the number of solar sails in formation, a different metric is defined to evaluate the quality of formation in terms of size and shape for two-craft, three-craft, and four-craft formations.

A nonlinear programming (NLP) approach is employed to design a drift-free, in-plane, two-craft formation of a specific size within the RoI. The word *in-plane* refers to the fact that both solar sails lie in the same orbit plane, which in this case is the ecliptic plane. A similar numerical approach is used to design in-plane equilateral triangle and regular tetrahedron formations, which are subsequently compared, in terms of formation quality and stability, to the formations flown in the MMS mission. In this paper, MATLAB's constrained minimization routine *fmincon*, with the *active-set* algorithm, is used to find a locally optimal solution. Note that the effects of repeated short-term eclipses are shown to be negligible for the orbit regime discussed in this study (McInnes et al., 2001), and therefore, short-term terrestrial shadows are ignored in the numerical simulations.

3.1. Two-craft formation

For a solar sail flying in a Sun-synchronous orbit, the average secular variations of orbital elements over a single orbit due to the SRP force in Eq. (5) are found to be (Parsay, 2016; Parsay and Schaub, 2017),

$$\dot{\bar{a}} = 0 \tag{9a}$$

$$\dot{\bar{e}} = 0 \tag{9b}$$

$$\dot{\bar{\omega}} = \frac{3k\sqrt{\bar{a}(1-\bar{e}^2)}}{2\bar{e}\sqrt{\mu}} \tag{9c}$$

$$\dot{\bar{M}} = \bar{n} - \frac{3\sqrt{\bar{a}}(1+\bar{e}^2)k}{2\bar{e}\sqrt{\mu}} \tag{9d}$$

For the relative motion of two solar sails in Sun-synchronous orbits to remain invariant to the relative effects of SRP, the following two secular drift rates must be matched,

$$\dot{\bar{\omega}}_d = \dot{\bar{\omega}}_c \tag{10a}$$

$$\dot{\bar{M}}_d = \dot{\bar{M}}_c \tag{10b}$$

As evident in Eq. (10), there are *two constraints* that the deputy states must satisfy for a SRP invariant relative motion with respect to a chief solar sail flying in a Sun-synchronous orbit. These two constraints are functions of *three variables* ($\bar{a}, \bar{e}$, and k). Therefore, there is only *one free variable* to choose; once a variable is chosen, the other two free variables are prescribed such that both SRP invariant conditions in Eq. (10) are satisfied. For instance, if the deputy solar sail has a fixed characteristic acceleration, there is only one unique orbit that the deputy can occupy that leads to a SRP invariant relative motion with respect to the chief flying in a Sun-synchronous orbit. The concept of SRP invariant relative orbits are analogous to J_2 invariant relative orbits that were introduced by Alfriend and Schaub (Schaub et al., 2000; Schaub and Alfriend, 2001; Schaub, 2003).

For the two-craft formation, the average inter-spacecraft range within the RoI is defined as the metric for evaluating the quality of a formation. The relative position vector between two solar sails at any point in time is written as,

$$\boldsymbol{\rho}(t) = \boldsymbol{r}_d(t) - \boldsymbol{r}_c(t) \tag{11}$$

The average distance between the two solar sails within the RoI is defined as,

$$\bar{\rho} = \frac{1}{N}\sum_{k=1}^{N}\rho_k \tag{12}$$

where $\rho_k = ||\boldsymbol{\rho}_k||$ and N is the number of integration steps within the RoI. Let l denote the sail's mean longitude, defined as,

$$l = \omega + M \tag{13}$$

The total relative change in mean longitude over an arbitrary number of complete revolutions is defined as,

$$\Delta l = \int_{t_0}^{t_f} \left(\dot{l}_d(t) - \dot{l}_c(t)\right)\mathrm{d}t \tag{14}$$

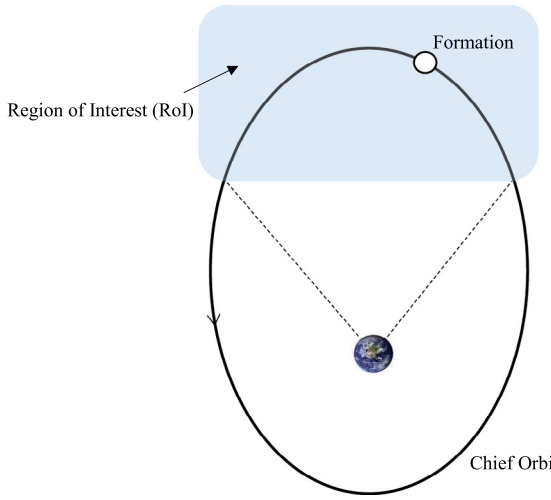

Fig. 3. Solar sail formation in a region of interest around apogee.

The variable Δl indicates how much the deputy has drifted apart with respect to the chief over a given time span. Given the chief's osculating elements $\mathfrak{oe}_{c_0}$, a two-craft formation design algorithm is proposed as follows,

$$\begin{aligned} \text{minimize} \quad & J = |\Delta l| \\ \text{with respect to} \quad & e_{d_0}, k_d, M_{d_0} \\ \text{subject to} \quad & \ddot{\boldsymbol{r}}_c = -\frac{\mu}{r_c^3}\boldsymbol{r}_c + \boldsymbol{a}_{s_c} \\ & \ddot{\boldsymbol{r}}_d = -\frac{\mu}{r_d^3}\boldsymbol{r}_d + \boldsymbol{a}_{s_d} \\ & \bar{\rho}_{\min} \leqslant \bar{\rho} \leqslant \bar{\rho}_{\max} \\ \text{free variables} \quad & a_{d_0}, \omega_{d_0} \end{aligned} \tag{15}$$

The choice of using Δl as the cost function for minimizing the relative drift is directly motivated by Eq. (10). Examples of the two-craft formation designed to maximize the science gain in the RoI are shown in Fig. 4 for the various formation sizes of 30, 180, and 300 km, in terms of average separation distance. The highlighted region represents the time that the formation is flying within the RoI. Each trajectory is propagated for 10 orbits. As evident in Fig. 4, the relative motion does not experience any relative drift in radial and along-track directions; it remains *invariant* to the relative effects of SRP perturbation.

3.2. Triangle formation

In this section, the desired three-craft formation geometry to be designed inside the RoI is a breathing in-plane equilateral triangle. The design of an out-of-plane triangle formation within a specified RoI has been discussed in the past (Parsay and Schaub, 2015), using a different algorithm. For this in-plane formation geometry, a preliminary

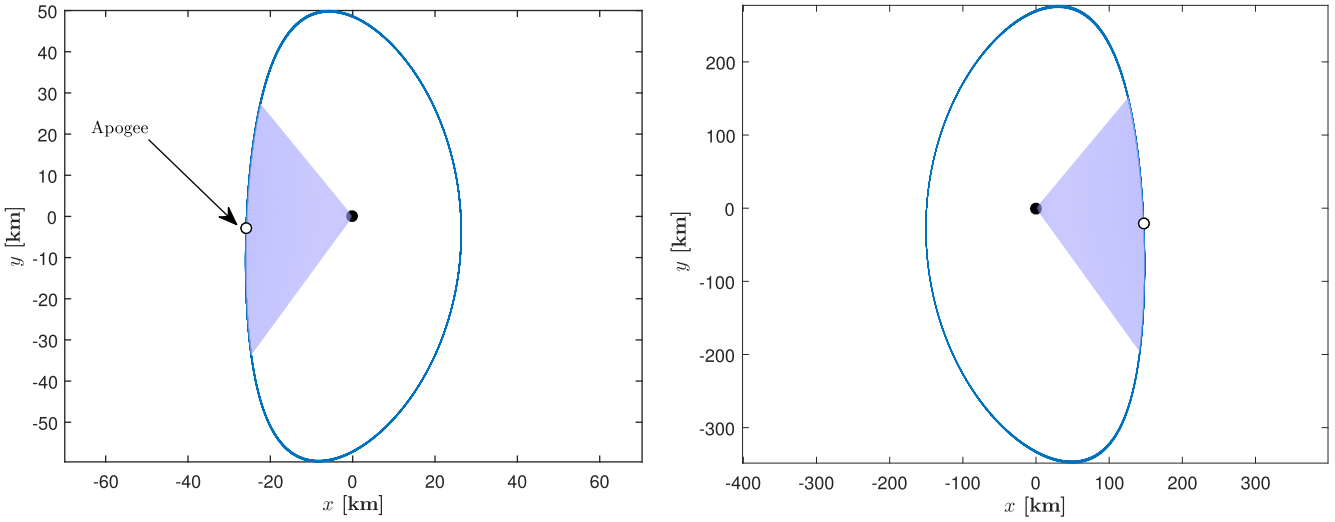

(a) 30 km formation

(b) 180 km formation

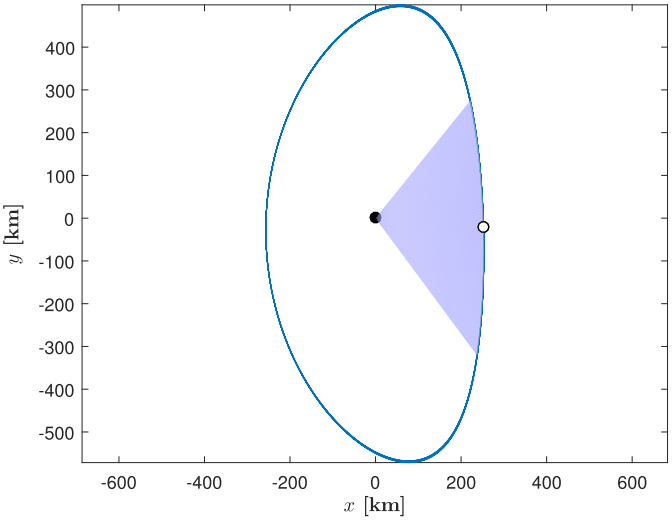

(c) 300 km formation

Fig. 4. Two-craft drift-free formation expressed in Chief's LVLH frame (radial vs. along-track).

formation is designed analytically. This preliminary formation is then used as an initial guess for the numerical algorithm to design a triangle inside the RoI. The initial step in designing a formation is to define a metric that measures the *quality* of formation. For the MMS mission, it is desired that the formation remains close to a regular tetrahedron for as long as possible within the RoI. MMS uses an instantaneous scalar metric called Quality Factor (Q) which measures both shape (Q_v) and size (Q_s) of tetrahedron formation with respect to a regular tetrahedron at any given time (Hughes, 2008a; Hughes et al., 2005; Hughes, 2008b; Mann et al., 2011). This formation quality metric is adapted in this paper to design triangle and tetrahedron formations. The use of the formation quality factor Q allows direct comparison to be made between the results in this paper and formations designed for the MMS mission. For a triangle formation, the quality factor is defined using,

$$Q(t) = Q_a(t)Q_s(t) \tag{16}$$

In order to define the scalar functions Q_a and Q_s explicitly, the following parameters need to be introduced. Each side of the triangle formation at any given time, $\boldsymbol{s}_j$, is defined as,

$$\begin{aligned} \boldsymbol{\rho}_1 &= \boldsymbol{r}_{d_1} - \boldsymbol{r}_c \\ \boldsymbol{\rho}_2 &= \boldsymbol{r}_{d_2} - \boldsymbol{r}_c \\ \boldsymbol{\rho}_3 &= \boldsymbol{r}_{d_1} - \boldsymbol{r}_{d_2} \end{aligned} \tag{17}$$

where $\boldsymbol{r}_c$, $\boldsymbol{r}_{d_1}$, $\boldsymbol{r}_{d_2}$ are the position vectors of chief, first deputy, and second deputy respectively. The area of the triangle formation is defined at any epoch via,

$$A(t) = \frac{1}{2}|\boldsymbol{\rho}_1 \times \boldsymbol{\rho}_2| \tag{18}$$

Given the inter-spacecraft range of $\rho_j = \|\boldsymbol{\rho}_j\|$, the average side-length for triangle formation is determined by

$$\overline{L} = \frac{1}{3}\sum_{j=1}^{3}\rho_j \tag{19}$$

The area of an equilateral triangle with an average side-length of $\overline{L}$ is,

$$A_r = \frac{\sqrt{3}}{4}\overline{L}^2 \tag{20}$$

The instantaneous metric $Q_a(t)$ for evaluating the shape of a triangle formation is defined as the ratio of the actual triangle area to the area of an equilateral triangle with averaged side-length of $\overline{L}$,

$$Q_a(t) = \frac{A}{A_r} \tag{21}$$

The size metric, Q_s, is a smooth piecewise function defined as,

$$Q_s(\overline{L}) = \begin{cases} 0 & \overline{L} < l_1 \\ \frac{(\overline{L}-l_1)^2(\overline{L}+l_1-2l_2)}{(l_2-l_1)^4} & l_1 \leqslant \overline{L} \leqslant l_2 \\ 1 & l_2 < \overline{L} \leqslant l_3 \\ \frac{(\overline{L}-l_4)^2(\overline{L}+l_4-2l_3)}{(l_4-l_3)^4} & l_3 < \overline{L} \leqslant l_4 \\ 0 & \overline{L} > l_4 \end{cases} \tag{22}$$

where $l_1, \cdots, l_4$ are constants in km that are chosen for every formation size in order to define the acceptable size range. These constants are tabulated in Table 1 for each of the formation sizes considered, which are the same values used in the formation design algorithm of the MMS mission.

The average value of the metric Q within the RoI at N number of integration steps is

$$\overline{Q}_{\text{RoI}} = \frac{1}{N}\sum_{k=1}^{N} Q_k \tag{23}$$

The average quality factor, $\overline{Q}_{\text{RoI}}$, must be maximized for a triangle formation to remain close to an equilateral triangle within the RoI. Thus, the cost function is chosen to be,

$$J_n = \overline{Q}_{\text{RoI}} \tag{24}$$

where n is the orbit number that the cost function is evaluated on. Having defined the cost function, the triangle formation design problem may be formulated as,

$$\begin{aligned} \text{minimize} \quad & J = -\sum_{n=1}^{N_{\text{orb}}} J_n \\ \text{with respect to} \quad & \Delta\boldsymbol{\alpha}_0 = \begin{bmatrix} \Delta a_{j_0} & \Delta e_{j_0} & \Delta\omega_{j_0} & \Delta M_{j_0} \end{bmatrix}^T \\ \text{subject to} \quad & \ddot{\boldsymbol{r}} = -\frac{\mu}{r^3}\boldsymbol{r} + \boldsymbol{a}_s \\ & \Delta i_{j_0} = 0, \Delta\Omega_{j_0} = 0 \\ & k_j = \frac{2}{3}\dot{\lambda}_s \frac{e_j}{\sqrt{1-e_j^2}}\sqrt{\frac{\mu}{a_j}} \end{aligned} \tag{25}$$

where N_{orb} is the total number of orbits that the average quality factor within the RoI is optimized over. Enforcing the characteristic acceleration value assures that each orbit remains Sun-synchronous.

To solve the NLP problem, a crude initial guess is designed analytically. This initial guess is a perfect equilateral triangle at the chief's apogee with the desired side-length $\overline{L}$. This *instantaneous* equilateral triangle is illustrated in Fig. 5. Given the chief's apogee radius of $\boldsymbol{r}_{a_c}$, the deputies' apogee radius are determined using,

Table 1
l_i ($i = 1, 2, 3, 4$) constants in $Q(s)$ function per formation size.

	10 km	30 km	60 km	160 km	400 km
l_1	4	19.3125	45	135	250
l_2	6	23.1500	50	140	300
l_3	18	42.0750	75	190	550
l_4	25	49.4750	80	210	600

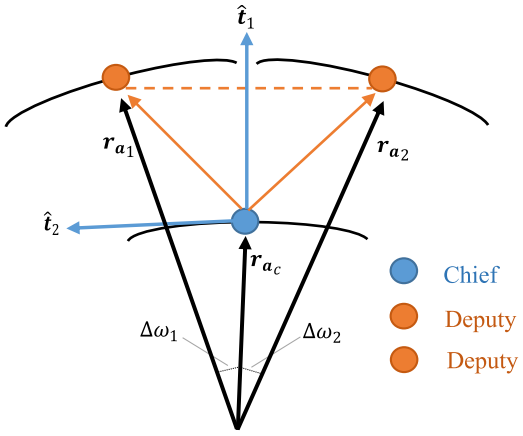

Fig. 5. Instantaneous equilateral triangle at Chief's apogee.

$$\boldsymbol{r}_{a_j} = \boldsymbol{r}_{a_c} + \boldsymbol{L}_j \tag{26}$$

where ${}^{\mathcal{T}}\boldsymbol{L}_j$ are the triangle sides expressed in a local frame $\mathcal{T} = \begin{bmatrix}\hat{\boldsymbol{t}}_1 & \hat{\boldsymbol{t}}_2 & \hat{\boldsymbol{t}}_3\end{bmatrix}$ that has its origin at the chief's position,

$${}^{\mathcal{T}}\boldsymbol{L}_1 = \begin{bmatrix}\frac{1}{2}\overline{L} & \frac{\sqrt{3}}{2}\overline{L} & 0\end{bmatrix}^T \tag{27a}$$

$${}^{\mathcal{T}}\boldsymbol{L}_2 = \begin{bmatrix}\frac{1}{2}\overline{L} & -\frac{\sqrt{3}}{2}\overline{L} & 0\end{bmatrix}^T \tag{27b}$$

The triangle frame $\mathcal{T}$ is defined with respect to the LVLH frame $\mathcal{O}$ via,

$$[\mathcal{O}\mathcal{T}] = [\boldsymbol{C}_1(\theta_1)][\boldsymbol{C}_2(\theta_2)][\boldsymbol{C}_3(\theta_3)] \tag{28}$$

For this initial guess, it is assumed that all solar sails have the same osculating semi-major axis at this instant and that they are all at their orbit apogee. Thus, the perigee radius for each spacecraft is computed by $r_{p_j} = 2a_c - r_{a_j}$ where $r_{a_j} = ||\boldsymbol{r}_{a_j}||$. The deputies' eccentricities are determined using their apogee and perigee radii. Because the formation's geometry of interest is an in-plane triangle, the deputies' inclinations and right ascension of ascending nodes are identical to those of the chief. The argument of perigee for each deputy is determined using,

$$\omega_{d_1} = \omega_c + \Delta\omega \tag{29a}$$

$$\omega_{d_2} = \omega_c - \Delta\omega \tag{29b}$$

where the differential element $\Delta\omega$ is,

$$\Delta\omega = \cos^{-1}\left(\frac{\boldsymbol{r}_{a_j}\cdot\boldsymbol{r}_{a_c}}{r_{a_j}r_{a_c}}\right) \tag{30}$$

Table 2
Initial guess for triangle orbital elements.

Chief	Deputy 1	Deputy 2
a_c	a_c	a_c
e_c	$\frac{r_{a_1}-r_{p_1}}{2a_c}$	$\frac{r_{a_2}-r_{p_2}}{2a_c}$
i_c	i_c	i_c
Ω_c	Ω_c	Ω_c
ω_c	$\omega_c + \Delta\omega$	$\omega_c - \Delta\omega$
$f_c = \pi$	f_c	f_c

The orbital elements for each spacecraft in this crude initial guess is summarized in Table 2. To determine the quality and stability of this formation, the formation is propagated for approximately 15 orbits. As evident in Fig. 6(c), the formation forms a perfect equilateral triangle at the orbit apogee but is immediately deformed after apogee, as is also shown by the sharp decrease in the formation quality factor Q. The average quality factor is approximately $\overline{Q}_{\text{RoI}} = 0.61$. This is far below the limit acceptable for a formation that is useful for collecting science data, but serves as an adequate initial guess for the numerical optimizer. The relative motion as seen by the chief's LVLH frame is illustrated in Fig. 6(a). The time history of inter-spacecraft ranges are shown in Fig. 6(e). There are no dangerous close approaches throughout the entire simulation. Note that the simulation is run for only 60 days, but the quality of the formation remains high for nearly a year if propagated forward for that long. The simulation is run for 60 days in this study, because, in practice, achieving the *perfect* desired relative states may be difficult without having high-thrust capability. The failure to achieve the exact desired relative states can cause an increase in the relative drift rates, which may, occasionally, require the deputy spacecraft to employ active control for adjusting its relative states.

The algorithm described in Eq. (25) is utilized to design in-plane equilateral triangle formations with various sizes. The selected formation sizes in terms of average side-lengths are 10, 60, 160, 400 km. The chosen formation sizes are directly motivated by the formation sizes that are used in the MMS mission. Fig. 6(b) illustrates the one-orbit optimized solution for the 10 km triangle formation. As illustrated in Fig. 6(d), the quality factor remains acceptable for at least 60 days. The minimum spacecraft range is around 10 km, indicating a safe formation for the entire simulation. Because the eccentricity of the optimized orbits are different, it requires each solar sail to have a slightly different characteristic accelerations according to the Sun-synchronous condition. For this formation, the required change in reflectivity is less than 0.02% for both deputies. This difference in characteristic acceleration may be achieved by *reflectivity modulation*, which was employed by the Interplanetary Kite-craft Accelerated by Radiation Of the Sun (IKAROS) mission launched by the Japan Aerospace Exploration Agency (JAXA) in 2010. To change the surface reflectance, liquid crystal panels on the sail are switched on to produce specular reflection and switched off to create diffuse reflection. With the capability of changing the sail's surface reflectivity, the characteristic acceleration of a sail can be adjusted (Mori et al., 2014). Figs. 10–12 show the optimized solutions for the 60, 160, and 400 km formations, respectively. Similar to the 10 km formation, the designed formations are stable for at least 60 days and do not experience any dangerous close approaches.

In all formations designed, there is a slow secular drift that leads to a slow degradation of the formation quality.

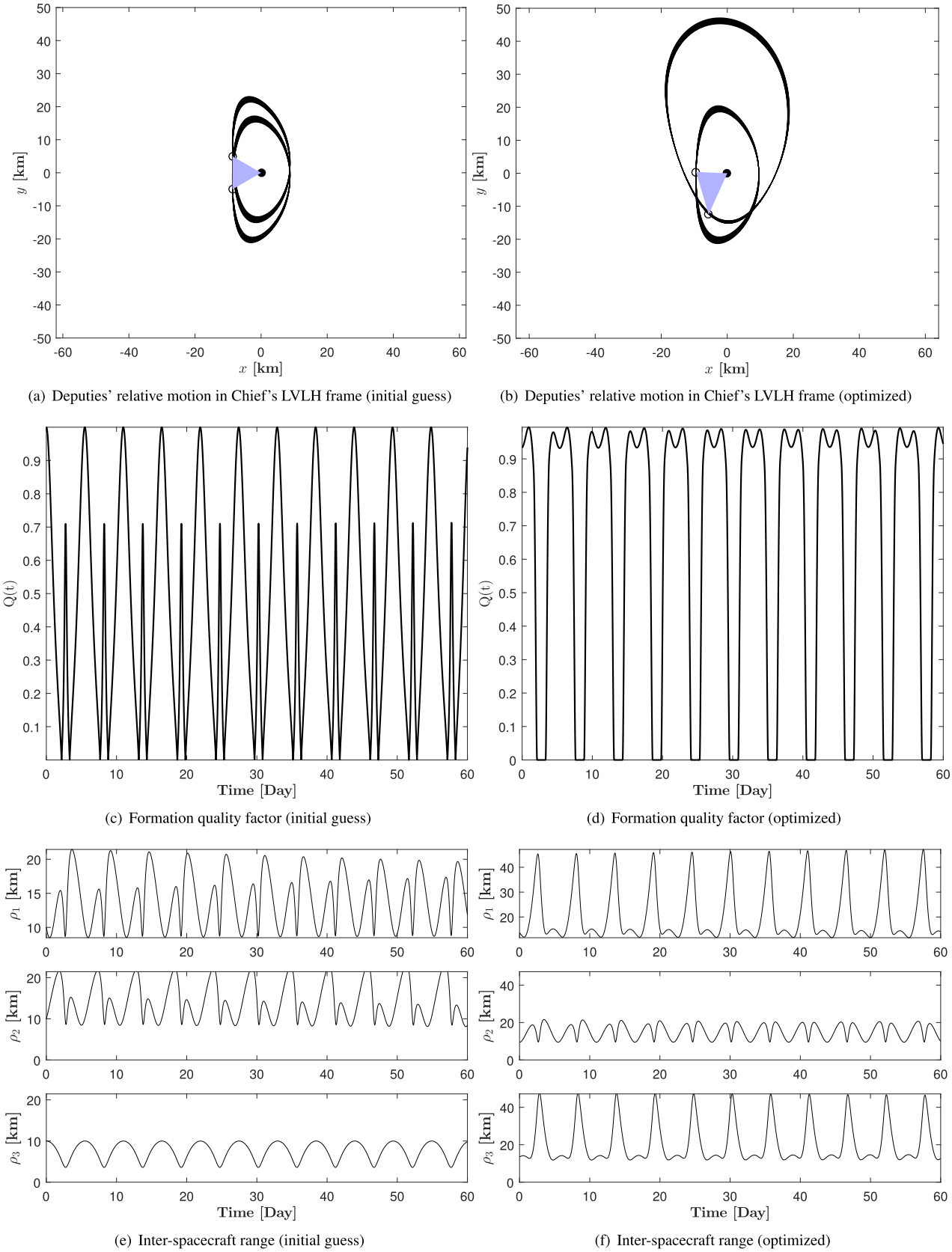

(a) Deputies' relative motion in Chief's LVLH frame (initial guess)

(b) Deputies' relative motion in Chief's LVLH frame (optimized)

(c) Formation quality factor (initial guess)

(d) Formation quality factor (optimized)

(e) Inter-spacecraft range (initial guess)

(f) Inter-spacecraft range (optimized)

Fig. 6. Initial guess vs. optimized solution for in-plane equilateral triangle formation design.

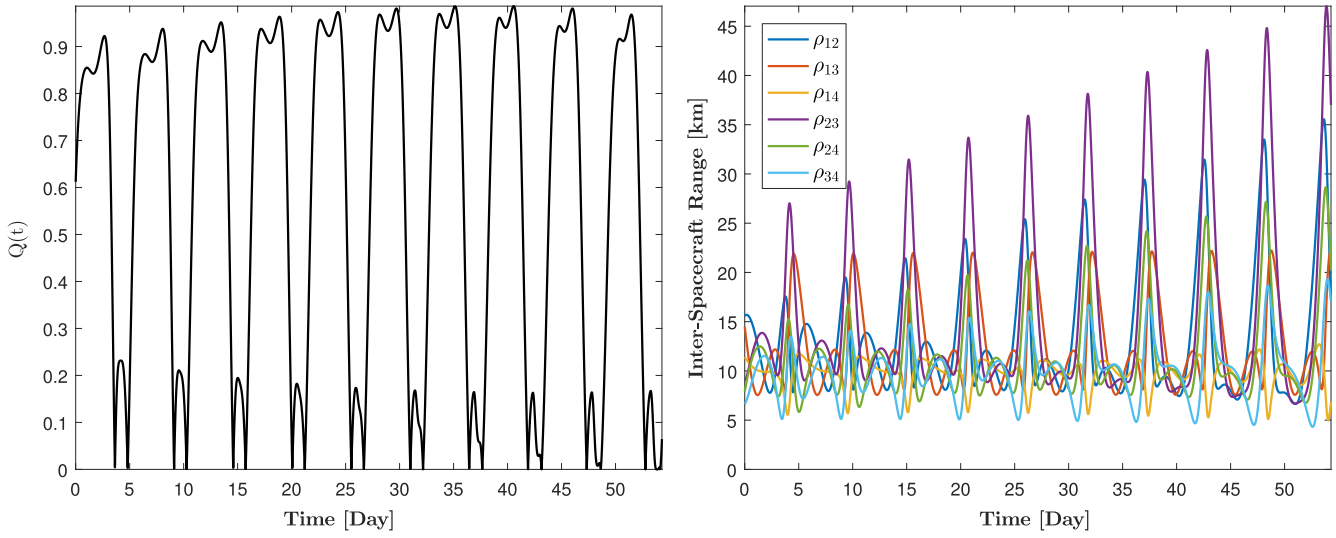

(a) Formation quality

(b) Inter-spacecraft range

Fig. 7. Tetrahedron formation with average side-length of 10 km (10 orbit optimized).

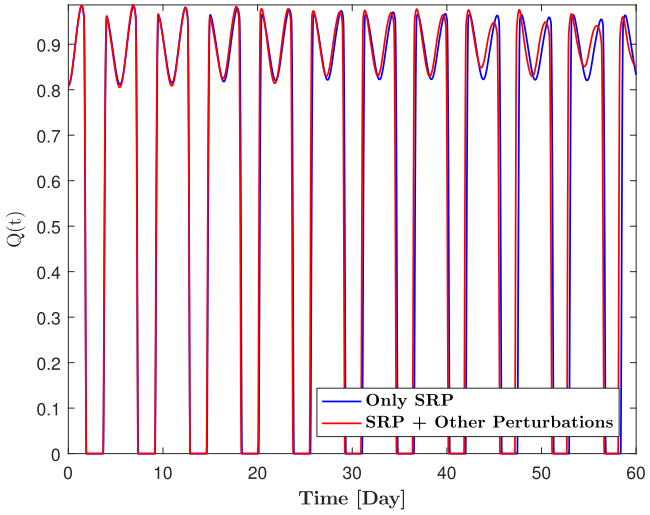

Fig. 8. Effects of perturbations on an optimal triangle formation.

The main reason for this apparent relative drift is the absence of enforcing the relative SRP invariant condition. As it can be seen from Eq. (25), the objective is to maximize the quality of the formation and there is no enforced constraint that involves minimizing the relative drifts between the solar sails. The inclusion of the relative SRP invariant condition is discussed in Section 3.5.

3.3. Tetrahedron formation

The minimum number of spacecraft to fully study the spatial and temporal changes of magnetic reconnection in three-dimensions is four (Burch et al., 2016). This section investigates the possibility flying four solar sails that form a tetrahedron within the RoI. The formation design problem is analogous to the triangle formation, with a modification in the cost function. For the shape metric, the volume metric, Q_v, is used as opposed to the area metric Q_a in the triangle formation design problem. Therefore, for the tetrahedron formation design, the instantaneous quality factor $Q(t)$ is defined as,

$$Q(t) = Q_v(t)Q_s(t) \tag{31}$$

The *actual* volume of tetrahedron formation at any given time is governed by

$$V(t) = \frac{1}{6}|\boldsymbol{\rho}_1 \cdot (\boldsymbol{\rho}_2 \times \boldsymbol{\rho}_3)| \tag{32}$$

The volume of a regular tetrahedron that has the same average side length of $\bar{L}$ is calculated through

$$V_r = \frac{\sqrt{2}}{12}\bar{L}^3 \tag{33}$$

The volume metric is defined as the ratio of the actual tetrahedron volume, V_a, to the volume of a regular tetrahedron V_r.

$$Q_v(t) = \frac{V}{V_r} \tag{34}$$

Both Q_v and Q_s have a range that falls between 0 and 1. Q_v will equal 1 when the volume of the tetrahedron equals that of a regular tetrahedron and it will be equal to 0 when all four spacecraft lie in a plane. Q_s will equal 1 when the formation falls within the desired size range and 0 when it is outside of the acceptable range. The NLP problem of designing tetrahedron solar sail formation may be written as,

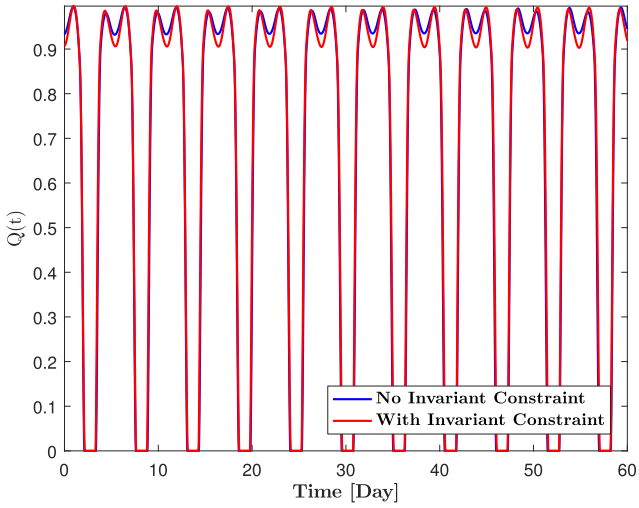

(a) Formation quality factor

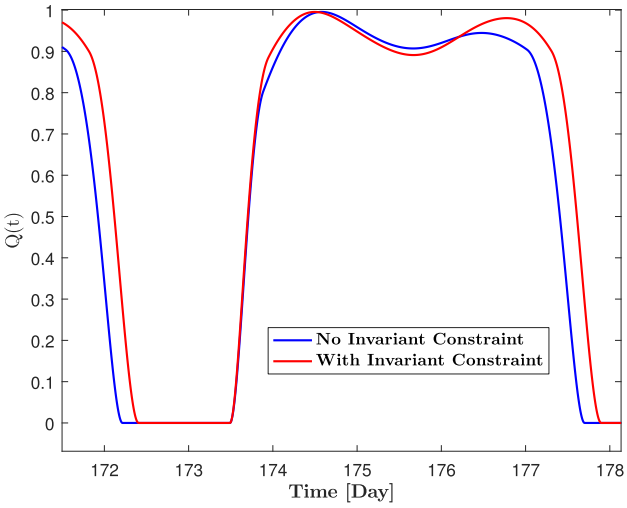

(b) Formation quality factor close-up

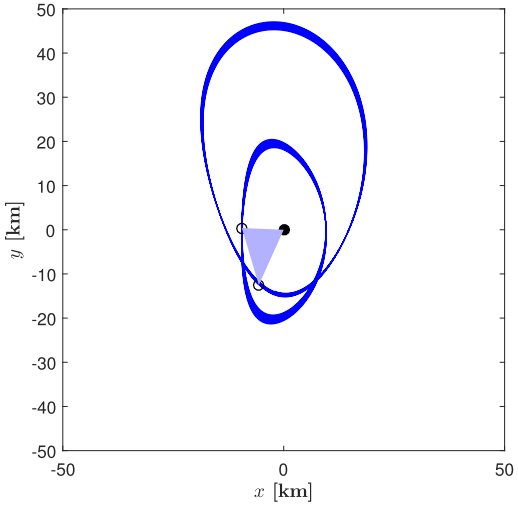

(c) Without constraint - 60 days propagation

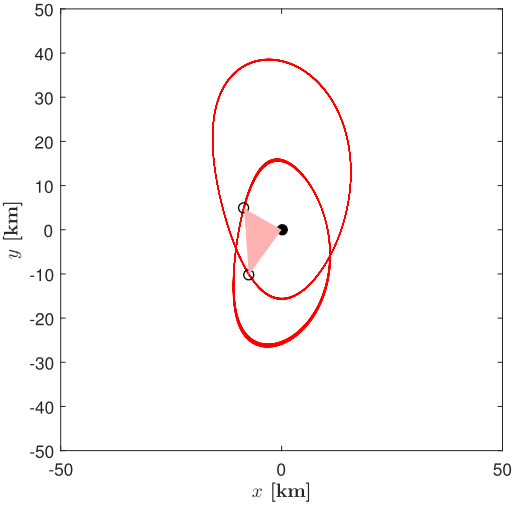

(d) With constraint - 60 days propagation

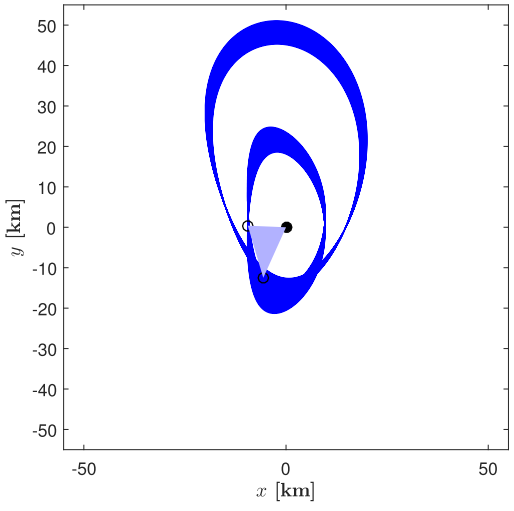

(e) Without constraint - 180 days propagation

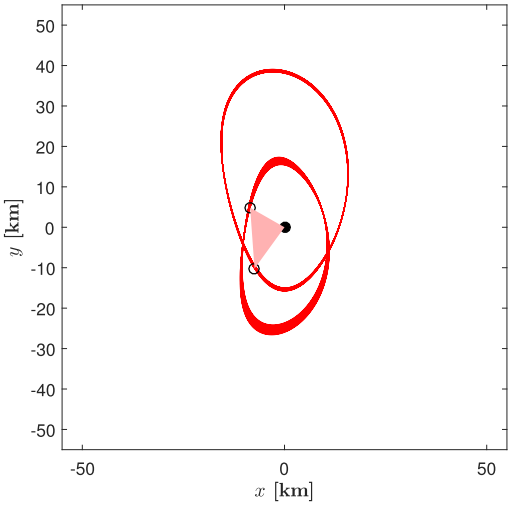

(f) With constraint - 180 days propagation

Fig. 9. Numerical inclusion of SRP invariant condition in triangle formation design.

$$\begin{aligned} \text{minimize} \quad & J = -\sum_{n=1}^{N_{\text{orb}}} J_n \\ \text{with respect to} \quad & \Delta\boldsymbol{\alpha}_0 = \left[\Delta a_{j_0}\ \Delta e_{j_0}\ \Delta i_{j_0}\ \Delta\Omega_{j_0}\ \Delta\omega_{j_0}\ \Delta M_{j_0}\right]^T \\ \text{subject to} \quad & \ddot{\boldsymbol{r}} = -\frac{\mu}{r^3}\boldsymbol{r} + \boldsymbol{a}_s \\ & k_j = \frac{2}{3}\dot{\lambda}_s \frac{e_j}{\sqrt{1-e_j^2}}\sqrt{\frac{\mu}{a_j}} \end{aligned} \tag{35}$$

A regular tetrahedron with side-length $\overline{L}$ is used as an initial guess for the numerical solver (Hughes et al., 2005; Hughes, 2008a; Hughes, 2008b). Assuming the chief is at the origin of a local frame $\mathcal{T}$, the deputies' relative position vectors expressed in $\mathcal{T}$ frame are

$${}^{\mathcal{T}}\boldsymbol{L}_1 = \begin{bmatrix} \overline{L} \\ 0 \\ 0 \end{bmatrix} \quad {}^{\mathcal{T}}\boldsymbol{L}_2 = \begin{bmatrix} \frac{1}{2}\overline{L} \\ \frac{\sqrt{3}}{2}\overline{L} \\ 0 \end{bmatrix} \quad {}^{\mathcal{T}}\boldsymbol{L}_3 = \begin{bmatrix} \frac{1}{2}\overline{L} \\ \frac{1}{2\sqrt{3}}\overline{L} \\ \sqrt{\frac{2}{3}}\overline{L} \end{bmatrix} \tag{36}$$

$$\boldsymbol{r}_{d_1} = \boldsymbol{r}_c + \boldsymbol{L}_1 \quad \boldsymbol{r}_{d_2} = \boldsymbol{r}_c + \boldsymbol{L}_2 \quad \boldsymbol{r}_{d_3} = \boldsymbol{r}_c + \boldsymbol{L}_3 \tag{37}$$

$$[\mathcal{OT}] = [\boldsymbol{C}_1(\theta_1)][\boldsymbol{C}_2(\theta_2)][\boldsymbol{C}_3(\theta_3)] \tag{38}$$

$$\boldsymbol{v}_{d_1} = v_1\hat{\boldsymbol{v}}_c \quad \boldsymbol{v}_{d_2} = v_2\hat{\boldsymbol{v}}_c \quad \boldsymbol{v}_{d_3} = v_3\hat{\boldsymbol{v}}_c \tag{39}$$

The velocities of the deputy spacecraft are assumed to have the same direction as the chief's velocity. The velocity magnitudes are computed through $v_j = \sqrt{2(\mathcal{E}_0 + \mu/r_j)}$, $j = 1, 2, 3$ where $\mathcal{E}_0 = -\mu/2a_c$. This crude initial guess is by no means optimal but provides a good starting point for the numerical solver. The Cartesian states of the deputies are converted to orbital elements and those initial differential orbital elements are passed to the numerical solver as an initial guess. An example of a 10-orbit optimized tetrahedron formation design is shown in Fig. 7. As evident from Fig. 7(a), the formation is useful for at least 10 orbits before it quickly degrades in the following orbits due to the relative out-of-plane variations. The inter-spacecraft ranges shown in Fig. 7(b) indicate that the tetrahedron formation has no dangerous close approaches between any of its spacecraft pairs throughout the 10-orbit period.

3.4. Effects of perturbations

As it can be seen from Eq. (25), the effects of perturbations besides SRP are ignored in the solution of the formation design problem. This is because the gravitational effects of the Earth and third-body effects of the Moon and Sun on the relative motion in this orbit regime are shown to be small based on the previous study (Parsay and Schaub, 2015). In Fig. 8, the optimal solution of a 160 km triangle formation is propagated with and without

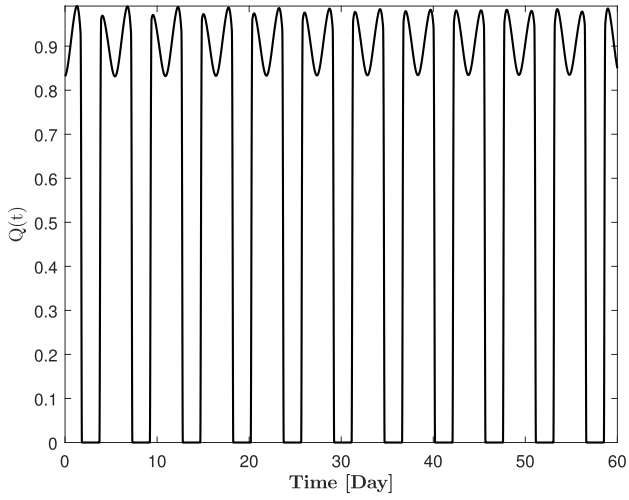

(a) Formation quality factor

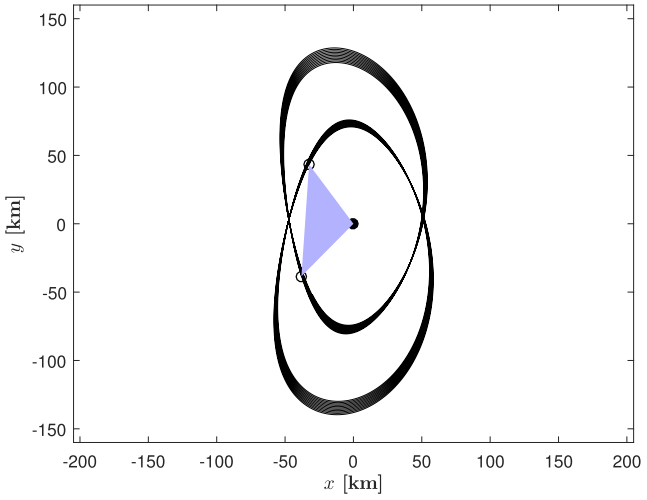

(b) Deputies' relative motion in Chief's LVLH frame

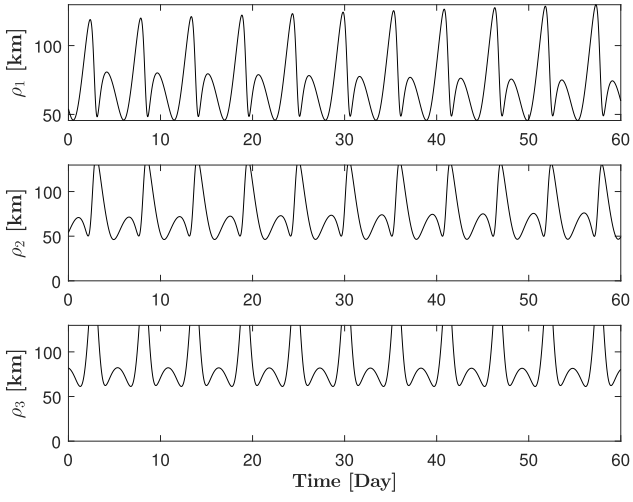

(c) Inter-spacecraft range

Fig. 10. In-plane equilateral triangle formation with average side-length of 60 km.

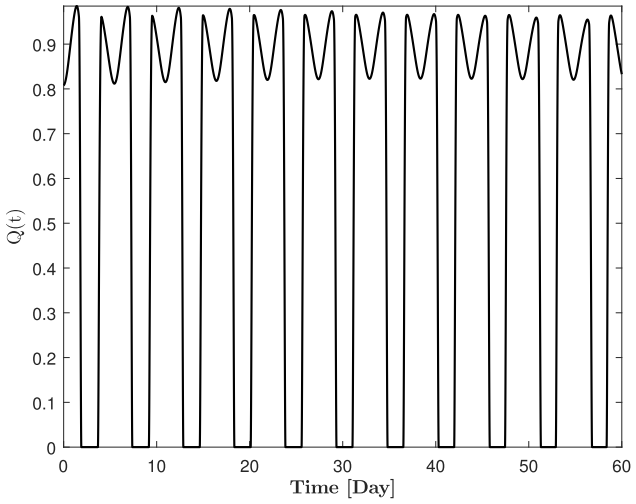

(a) Formation quality factor

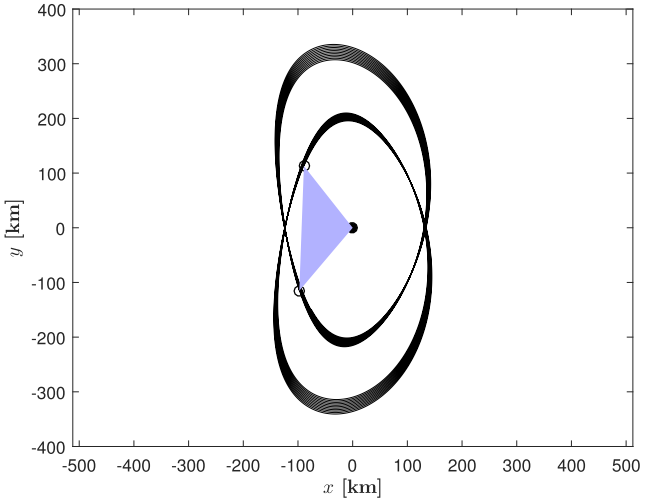

(b) Deputies' relative motion in Chief's LVLH frame

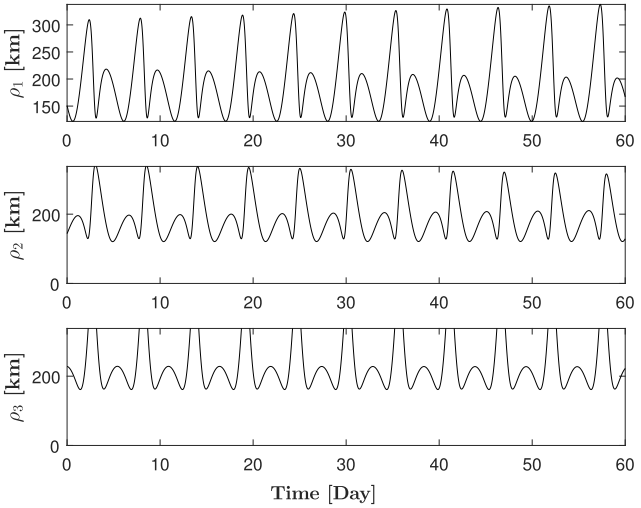

(c) Inter-spacecraft range

Fig. 11. In-plane equilateral triangle formation with average side-length of 160 km.

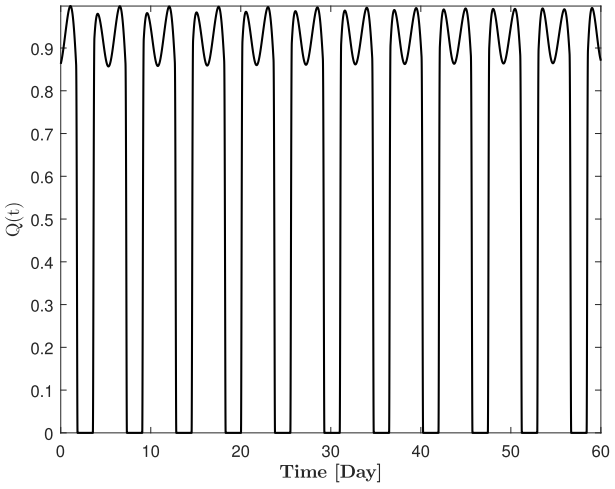

(a) Formation quality factor

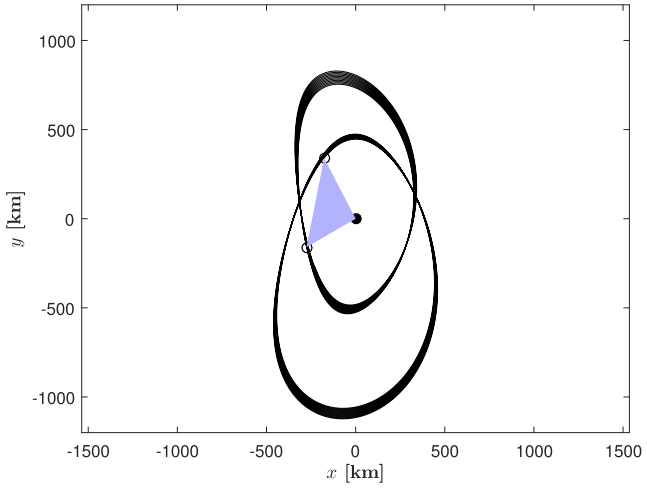

(b) Deputies' relative motion in Chief's LVLH frame

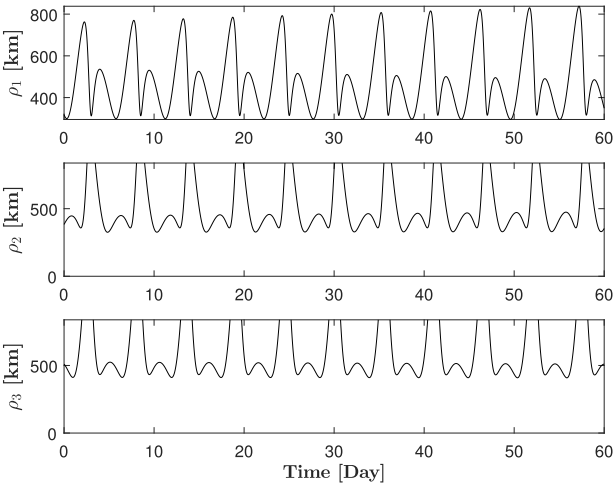

(c) Inter-spacecraft range

Fig. 12. In-plane equilateral triangle formation with average side-length of 400 km.

the inclusion of other perturbations. As evident, the effects of perturbations on the relative motion is negligible and the quality factor, $Q(t)$, remains above 0.8 for at least 60 days, which satisfies MMS mission requirements.

3.5. Numerical Inclusion of SRP invariant condition

As evident from Eqs. (25) and (35), there is no constraint that leads to the minimization of the relative drift between the solar sails. The question that arises is whether minimizing the relative drift has any effect on the long-term stability of the formation. Another valid question is whether the formation stability can be improved without sacrificing formation quality. To investigate these questions, the numerical algorithm is modified to include a constraint on how much the deputy spacecraft are allowed to drift apart over the span of the optimization. The modified algorithm is summarized as follows for the triangle formation,

$$\begin{aligned}
&\text{minimize} && J = -\sum_{n=1}^{N_{\text{orb}}} J_n \\
&\text{with respect to} && \Delta\mathbf{oe}_0 = \begin{bmatrix}\Delta a_{j_0} & \Delta e_{j_0} & \Delta\omega_{j_0} & \Delta M_{j_0}\end{bmatrix}^T \\
&\text{subject to} && \ddot{\boldsymbol{r}} = -\frac{\mu}{r^3}\boldsymbol{r} + \boldsymbol{a}_s \\
& && \Delta i_{j_0} = 0, \Delta\Omega_{j_0} = 0 \\
& && k_j = \frac{2}{3}\dot{\lambda}_s \frac{e_j}{\sqrt{1-e_j^2}}\sqrt{\frac{\mu}{a_j}} \\
& && \Delta l_{\min} \leqslant \Delta l_j \leqslant \Delta l_{\max}
\end{aligned} \tag{40}$$

An optimized 10 km triangle formation resulting from Eq. (40) is illustrated in Fig. 9. As shown in Fig. 9(a), the formation quality factor is slightly lower for the case where the relative SRP invariant condition is enforced. However, the formation quality factor degrades at a faster rate for the formation with no constraint on the relative drift, as evident in Fig. 9(b). The relative trajectories of the deputies with respect to the chief solar sail are illustrated in Fig. 9(e) and (f), corresponding to the case without the constraint and the case with the relative drift constraint, respectively. With the numerical inclusion of the invariance condition, the formation stability is improved at the price of a small decrease in the formation quality.

4. Conclusion

In this paper, the problem of solar sail formation design is explored in detail using numerical optimization for two-craft, three-craft, and four-craft formations. First, the design of truly SRP invariant solar sail formations within a specific region of interest around the orbit apogee are explored for the two-craft formation. Motivated by NASA's MMS mission, the problem of three-craft and four-craft formation design is subsequently investigated. The proposed algorithm is applied to the design of in-plane equilateral triangle and tetrahedron formations. Various formation sizes ranging from 10 km to 400 km in terms of average inter-spacecraft range are explored. It is shown that the in-plane solar sail formation geometries are stable, while the tetrahedron formation is difficult to design, assuming the fixed Sun-pointing attitude. Despite the long-term stability of the designed formations, active control may be necessary to adjust the formation sporadically, especially if there is a failure to achieve the desired states due to control accuracy and navigation errors. Finally, it is shown that the formations designed with the inclusion of relative drift constraints are more stable and degrade at a lower rate. This increase in formation stability may come with a small penalty in the quality of the designed formation.

References

Burch, J., Moore, T., Torbert, R., Giles, B., 2016. Magnetospheric multiscale overview and science objectives. Space Sci. Rev. 199 (1–4), 5–21. http://dx.doi.org/10.1007/s11214-015-0164-9.

Curtis, S., The Magnetospheric Multiscale Mission...Resolving Fundamental Processes in Space Plasmas.

Evans, D.S., Moore, T.E., 1979. Precipitating electrons associated with the diffuse aurora: evidence for electrons of atmospheric origin in the plasma sheet. J. Geophys. Res.: Space Phys. 84 (A11), 6451–6457. http://dx.doi.org/10.1029/JA084iA11p06451.

Gong, S., Yunfeng, G., Li, J., 2011. Solar sail formation flying on an inclined earth orbit. Acta Astronaut. 68 (1), 226–239. http://dx.doi.org/10.1016/j.actaastro.2010.08.022.

Hughes, S.P., 2008a. General method for optimal guidance of spacecraft formations. J. Guid. Control Dyn. 31 (2), 414–423. http://dx.doi.org/10.2514/1.23731.

Hughes, S.P., 2008b. Formation design and sensitivity analysis for the Magnetospheric Multiscale Mission (MMS). In: AIAA/AAS Astrodynamics Specialist Conference, Honolulu, HI.

Hughes, S.P., 2005. A Simple, Powerful Method for Optimal Guidance of Spacecraft Formations, Tech. Rep., NASA Goddard Space Flight Center.

Khazanov, G., Tripathi, A., Sibeck, D., Himwich, E., Glocer, A., Singhal, R., 2015. Electron distribution function formation in regions of diffuse aurora. J. Geophys. Res.: Space Phys. 120 (11), 9891–9915. http://dx.doi.org/10.1002/2015JA021728.

Macdonald, M., McInnes, C., 2005. Analytical control laws for planet-centered solar sailing. J. Guid. Control Dyn. 28 (5), 1038–1048. http://dx.doi.org/10.2514/1.11400.

Macdonald, M., Hughes, G., McInnes, C., Lyngvi, A., Falkner, P., Atzei, A., 2007. GeoSail: an elegant solar sail demonstration mission. J. Spacecraft Rock. 44 (4), 784–796. http://dx.doi.org/10.2514/1.22867.

Mann, L., Parsay, K., Williams, T., Yu, W., 2011. Comparison of Magnetospheric MultiScale (MMS) formation design algorithms. In: 4th International Conference on Formation Flying, Montreal QUEBEC.

McInnes, C.R., 2004. Solar Sailing: Technology, Dynamics and Mission Applications. Springer.

McInnes, C.R., MacDonald, M., Angelopolous, V., Alexander, D., 2001. GeoSail: exploring the geomagnetic tail using a small solar sail. J. Spacecraft Rock. 38 (4), 622–629. http://dx.doi.org/10.2514/2.3727.

Moore, T., Khazanov, G., Mechanisms of ionospheric mass escape. J. Geophys. Res.: Space Phys. 115(A12). doi:http://dx.doi.org/10.1029/2009JA014905.

Mori, O., Shirasawa, Y., Mimasu, Y., Tsuda, Y., Sawada, H., Saiki, T., Yamamoto, T., Yonekura, K., Hoshino, H., Kawaguchi, J., et al.,

2014. Overview of IKAROS mission. In: Advances in Solar Sailing. Springer, pp. 25–43.

Mu, J., Gong, S., Li, J., 2014. Coupled control of reflectivity modulated solar sail for GeoSail formation flying. J. Guid. Control Dyn. 38 (4), 740–751. http://dx.doi.org/10.2514/1.G000117.

Parsay, K., 2016. Invariant Solar Sail Formations in Elliptical Sun-Synchronous Orbits Ph.D. thesis. University of Colorado (Boulder).

Parsay, K., Schaub, H., 2015. Designing solar sail formations in sun-synchronous orbits for geomagnetic tail exploration. Acta Astronaut. 107, 218–233. http://dx.doi.org/10.1016/j.actaastro.2014.11.018.

Parsay, K., Schaub, H., 2017. Drift-free solar sail formations in elliptical Sun-synchronous orbits. Acta Astronaut. 139, 201–212. http://dx.doi.org/10.1016/j.actaastro.2017.06.027.

Schaub, H., 2003. Incorporating secular drifts into the orbit element difference description of relative orbits. Adv. Astronaut. Sci. 114, 239–257.

Schaub, H., Alfriend, K.T., 2001. J2 invariant relative orbits for spacecraft formations. Celestial Mech. Dyn. Astron. 79 (2), 77–95. http://dx.doi.org/10.1023/A:1011161811472.

Schaub, H., Vadali, S.R., Junkins, J.L., Alfriend, K.T., 2000. Spacecraft formation flying control using mean orbit elements. J. Astronaut. Sci. 48 (1), 69–87.

Strangeway, R., Ergun, R., Su, Y.-J., Carlson, C., Elphic, R., Factors controlling ionospheric outflows as observed at intermediate altitudes. J. Geophys. Res.: Space Phys. 110(A3). doi:http://dx.doi.org/10.1029/2004JA010829.